AGU PUBLICATIONS

Water Resources Research

RESEARCH ARTICLE
10.1002/2014WR016508

Companion to *Queloz et al.* [2015], doi:10.1002/2014WR016433

Key Points:
- Travel time distributions are not stationary
- Forward and backward travel time distributions are different
- Nonstationary travel time distributions reproduce tracer data

Correspondence to:
E. Bertuzzo,
enrico.bertuzzo@epfl.ch

Citation:
Queloz, P., L. Carraro, P. Benettin, G. Botter, A. Rinaldo, and E. Bertuzzo (2015), Transport of fluorobenzoate tracers in a vegetated hydrologic control volume: 2. Theoretical inferences and modeling, *Water Resour. Res.*, *51*, 2793–2806, doi:10.1002/2014WR016508.

Received 5 OCT 2014
Accepted 19 MAR 2015
Accepted article online 24 MAR 2015
Published online 26 APR 2015

Transport of fluorobenzoate tracers in a vegetated hydrologic control volume: 2. Theoretical inferences and modeling

Pierre Queloz[1], Luca Carraro[1,2], Paolo Benettin[2], Gianluca Botter[2], Andrea Rinaldo[1,2], and Enrico Bertuzzo[1]

[1]Laboratory of Ecohydrology, Ecole Polytechnique Fédérale de Lausanne, Lausanne, Switzerland, [2]DICEA, University of Padova, Padova, Italy

Abstract A theoretical analysis of transport in a controlled hydrologic volume, inclusive of two willow trees and forced by erratic water inputs, is carried out contrasting the experimental data described in a companion paper. The data refer to the hydrologic transport in a large lysimeter of different fluorobenzoic acids seen as tracers. Export of solute is modeled through a recently developed framework which accounts for nonstationary travel time distributions where we parameterize how output fluxes (namely, discharge and evapotranspiration) sample the available water ages in storage. The relevance of this work lies in the study of hydrologic drivers of the nonstationary character of residence and travel time distributions, whose definition and computation shape this theoretical transport study. Our results show that a large fraction of the different behaviors exhibited by the tracers may be charged to the variability of the hydrologic forcings experienced after the injection. Moreover, the results highlight the crucial, and often overlooked, role of evapotranspiration and plant uptake in determining the transport of water and solutes. This application also suggests that the ways evapotranspiration selects water with different ages in storage can be inferred through model calibration contrasting only tracer concentrations in the discharge. A view on upscaled transport volumes like hillslopes or catchments is maintained throughout the paper.

1. Introduction

The concept of travel time has often been used in hydrology to characterize and model solute transport processes within hillslopes, aquifers, or catchments [e.g., *Kreft and Zuber*, 1978; *Jury et al.*, 1986; *Maloszewski et al.*, 1992; *Haggerty et al.*, 2002]. However, only recently the travel time literature evolved so as to include a detailed and realistic representation of the processes that drive solute circulation through the hydrologic response. Traditional approaches such as the lumped convolution approach [e.g., *Rodhe et al.*, 1996; *Kirchner et al.*, 2000; *Broxton et al.*, 2009; *McGuire and McDonnell*, 2006; *Seeger and Weiler*, 2014] were progressively made more general to account for the inherent time variability of fluxes and storages [*Botter et al.*, 2010; *Hrachowitz et al.*, 2009, 2010; *Heidbüchel et al.*, 2013; *Ali et al.*, 2014], which underlies the key differences between backward and forward distributions in hydrologically meaningful control volumes [*Niemi*, 1977; *Rinaldo et al.*, 2011; *Cvetkovic et al.*, 2012; *Harman*, 2015]. Similarly, the formalization of the differences and relationships between travel and residence time distributions [*Botter et al.*, 2011; *van der Velde et al.*, 2012] opened the way to a spatially integrated representation of the age-selection processes operated by bulk hydrologic fluxes like discharge and evapotranspiration. The approach complemented newly available high frequency data sets [e.g., *Kirchner and Neal*, 2013], which offered the opportunity to develop new methods and test novel modeling approaches to real-world transport problems [*van der Velde et al.*, 2010; *Heidbuchel et al.*, 2012; *Birkel et al.*, 2012; *McMillan et al.*, 2012; *Hrachowitz et al.*, 2013; *Davies et al.*, 2013; *Harman and Kim*, 2014; *van der Velde et al.*, 2014; *Harman*, 2015].

In this paper, we make use of a general transport model [*Botter et al.*, 2010, 2011; *Rinaldo et al.*, 2011; *Bertuzzo et al.*, 2013; *Benettin et al.*, 2013a] to gain insight on data gathered during a controlled experiment which is described in a companion paper [*Queloz et al.*, 2015]. The experiment provides direct observational evidence of the nonstationary character of transport processes in a controlled hydrologic transport volume and highlights the key role of plant uptake and degradation processes for solute circulation dynamics.

The significance of the present work lies in the comparative assessment of the current needs for practical modeling tools that reconcile recent theoretical advances with field experiments—which is one of the main goals of this paper.

Despite the small spatial scale used in the experiment, our modeling task may be considered equally significant and challenging as larger catchment studies. Indeed, transport processes are herein modeled using bulk measurements (output and input fluxes and storage mass at any time) of the same type of those that can possibly be measured or inferred at catchment scale [e.g., *Brutsaert and Nieber*, 1977; *Kirchner*, 2009; *Botter et al*., 2009]. Moreover, at catchment scale, the overall effect of heterogeneous attributes may be smoothed when integrated fluxes are dealt with, thereby easing a robust description of any flow path heterogeneity within the travel time formulation of transport [*Dagan*, 1988; *Botter et al*., 2005; *Cvetkovic et al*., 2012]. Significantly, the experiment retains key features of field studies like the random nature of rainfall (which was added as a sequence of quasi-instantaneous inputs) and the structural difference between the sampling of stored water particles operated by plant roots and drainage structures. On the other hand, transport features that can possibly emerge at hillslope and catchment scales, e.g., those induced by dynamically changing hydrological connectivity, cannot be investigated in this experiment. Despite these limitations, modeling the outcome of a lysimeter experiment of the type handled here is deemed a challenging test for our theoretical framework.

The paper is organized as follows. Section 2.1 illustrates the experiment and the data set available. Sections 2.2 and 2.3 present the modeling framework while the application to the lysimeter experiment is described in section 2.4. Section 3 presents the results that are then discussed in section 4. A section of conclusions, with a view on upscaled transport volumes like hillslopes or catchments, closes the paper.

2. Methods

2.1. Experimental Data

Hydrological time series and tracer breakthrough curves were recorded during a large lysimeter experiment running from April 2013 to July 2014. A detailed description of the setup and discussion of the experimental data are reported in a companion paper [*Queloz et al*., 2015]. A 2 m deep, 1 m^2 surface area lysimeter was filled with a sandy clay loam soil and planted with two willow stems (*Salix viminalis*). A 50 cm saturated gravel filter drains infiltration water to the outlet equipped with discharge flow measurement and flow-rated sampling system. A translucent roof located beneath the canopy protects the lysimeter surface from natural precipitation; instead, random rainfall following a marked Poisson process [*Rodriguez-Iturbe et al*., 1999] was manually injected. Load cells provide an accurate reading of the weight of the system and therefore allow the indirect estimate of evapotranspiration fluxes. Five selected rainfall events in the beginning of the experiment were each marked with a different tracer (various fluorobenzoic acids) that can be easily quantified in water samples using mass spectrometry techniques. Extensive discharge flow sampling was performed to precisely record the tracer breakthrough curves and calculate the outgoing tracer mass flux. A conceptual scheme of the lysimeter is reported in Figure 1a. The data set used in this paper is summarized in Figure 1b.

2.2. Travel Time Formulation of Transport and Age-Selection Schemes

Let us consider a hydrologic control volume with a single input flux J (e.g., precipitation) and two output fluxes: discharge Q and evapotranspiration ET. The proposed framework could be readily generalized to model more complex schemes involving multiple control volumes (in series or in parallel) [see e.g., *Bertuzzo et al*., 2013; *Benettin et al*., 2013a] or multiple input/output fluxes (e.g., irrigation and pumping). We first illustrate the theoretical approach for the simple case of a single control volume. The residence time T (also termed age) of a tagged water particle in storage within the control volume is defined as the time elapsed since its entrance in the control volume. Therefore, the residence time distribution (RTD) $p_S(T,t)$—the probability density function of the residence time of the water particles contained in the control volume at time t [*Botter et al*., 2011]—characterizes at any time the age composition of the storage. The residence time of a particle that leaves the system as Q or ET is termed travel time (also known as transit time). The corresponding travel time distributions (TTDs) can be seen either as forward ($\vec{p}_Q(T,t_i)$, $\vec{p}_{ET}(T,t_i)$) or backward ($\overleftarrow{p}_Q(T,t)$, $\overleftarrow{p}_{ET}(T,t)$) distributions [*Niemi*, 1977; *Rinaldo et al*., 2011; *Cvetkovic et al*., 2012]. In the former case, the age distribution refers to the set of particles that simultaneously

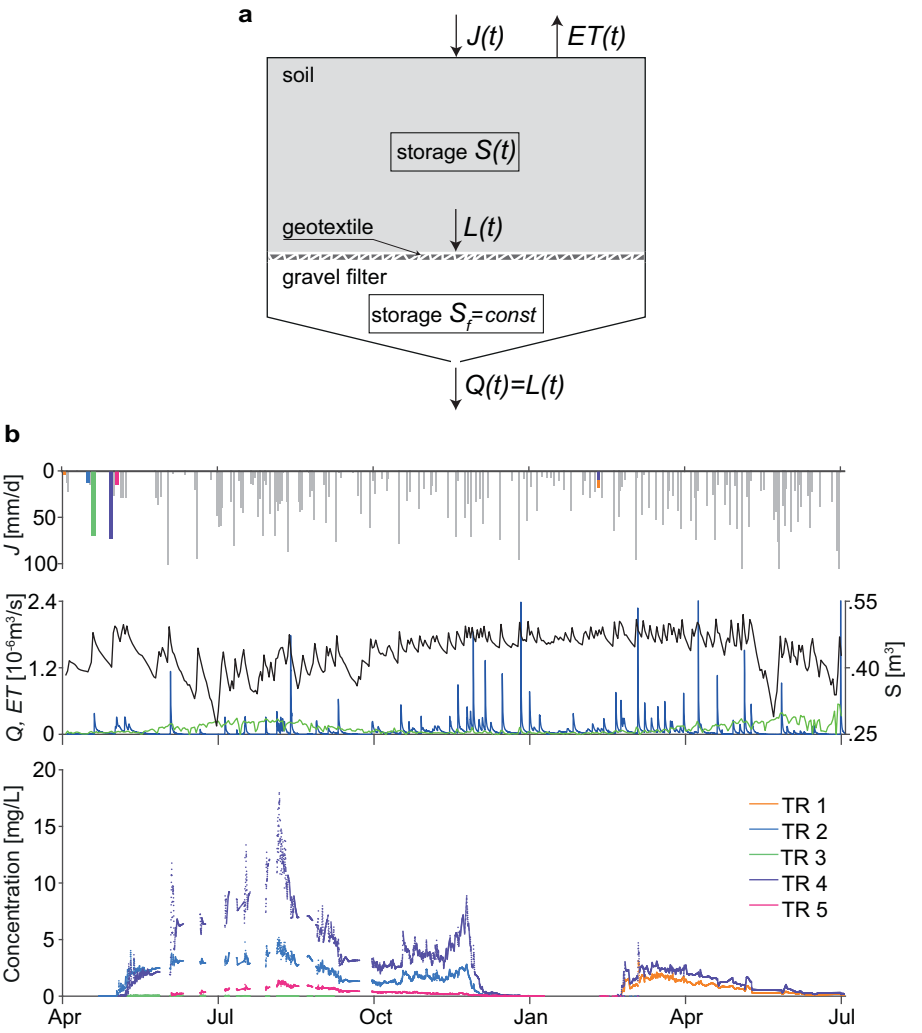

Figure 1. (a) Conceptual scheme of the lysimeter. From a modeling viewpoint, the system is divided into two control volumes: a 2 m deep, 1 m^2 surface area soil layer and a 50 cm deep gravel filter. We term precipitation input as $J(t)$, evapotranspiration as $ET(t)$, flow at the interface between soil and filter as $L(t)$, and bottom outflow as $Q(t)$. The system setup does not allow changes in water storage of the filter, therefore $Q(t)=L(t)$. (b) Time series of hydrological and chemical variables. (top) The rainfall pulses marked with the five different tracers are displayed with different colors. (bottom) Their breakthrough curves are displayed with the corresponding color. (middle) The time series of water storage S (black), outflow Q (blue), and ET (green).

entered the system at a time t_i, while in the latter case, the age distribution pertains to the set of particles that are simultaneously leaving the system at time t. The forward TTD can be thought as the flux in the outflow corresponding to an instantaneous marked injection of a unit volume at time t_i. The backward TTD represents instead the age distribution of the water sampled in the outflow at time t. If $\theta(t_i)$ is defined as the fraction of the precipitation influx $J(t_i)$ that ends up exiting as outflow Q, continuity and *Niemi* [1977] yield [*Botter et al.*, 2011]:

$$\overleftarrow{p}_Q(t-t_i,t)Q(t) = \theta(t_i)J(t_i)\overrightarrow{p}_Q(t-t_i,t_i)\,, \tag{1}$$

whose physical meaning consists of equating the fraction of particles that exits as Q at time t with age $t-t_i$ (at left-hand side) to the fraction of rainfall entered at t_i that exits as Q at time t (at right-hand side [RHS]). An analogous relation can be written for evapotranspiration TTDs.

Tracking the temporal evolution of the ages of the water particles stored within the control volume requires the specification of how outgoing fluxes sample the available ages in the storage. This is usually done by specifying the relationship between residence and backward TTDs through suitable selection functions [*Botter et al.*, 2011; *Botter*, 2012; *Benettin et al.*, 2013b]. Recently, *van der Velde et al.* [2012] proposed to

characterize age-selection processes by expressing the relevant distributions not as a function of age T but rather using a ranked age P_S that expresses the relationship between a certain age and all the other ages actually in storage. Specifically, the new variable $0 \leq P_S(T,t) \leq 1$ represents the fraction of storage younger than T at a given time t, and it is defined by the following equation:

$$P_S(T,t) = \int_0^T p_S(\tau,t)d\tau\,. \tag{2}$$

Therefore, at every time, there exists a unique relation between T and P_S which allows backward TTDs to be expressed in the domain of the new variable P_S: $\overleftarrow{p}_Q(T,t) \mapsto \overleftarrow{\omega}_Q(P_S,t)$ and $\overleftarrow{p}_{ET}(T,t) \mapsto \overleftarrow{\omega}_{ET}(P_S,t)$. $\overleftarrow{\omega}(P_S(T,t),t)$ are derived distributions (i.e., distributions of a function of the random variable T) and are termed "StorAge Selection" (SAS) functions because they determine how the resident ages are selected by the outflows. Once SAS functions are specified, the related time-variant RTDs and TTDs can be derived accordingly (see below).

The advantages of modeling age-selection through the transformed variable P_S are manifold. P_S can assume values between 0 and 1, corresponding to the youngest and the oldest storage in the system, respectively. Therefore, the support of the distribution $\overleftarrow{\omega}_Q(P_S,t)$ is also fixed and equal to the interval [0, 1]. $\overleftarrow{\omega}_Q(P_S,t)$ is a probability distribution function and can be parameterized. In forward modeling, it is therefore possible to specify directly the SAS functions to characterize how the output fluxes (Q and ET) select the different ages available within the control volume and derive the corresponding backward TTDs. Moreover, the ranked age P_S arguably embodies a better proxy of the position of a particle within the system [*van der Velde et al.*, 2012]—where the position should not depend on the actual value of the particle age but rather on the fraction of older particles stored within the system. In turn, the particle position in soil columns and hillslopes may strongly control the probability of being routed to the outflow or uptaken by plants.

As highlighted by the notation, the distributions $\overleftarrow{\omega}(P_S,t)$ can be time variant to mirror the variability in time of age-selection processes ruled by the outflows, e.g., depending on the external forcings and on the state of the system. However, even if a constant SAS function is assumed ($\overleftarrow{\omega}(P_S,t) = \overleftarrow{\omega}(P_S)$), the framework would consistently produce time-variant TTDs because the RTD (and thus the relation between T and P_S, see equation (2)) is also time variant.

A graphical representation of the modeling framework is presented in Figure 2. White bars in Figure 2a sketch an RTD as a function of the residence time T at a certain time t. We use a histogram to illustrate the actual numerical implementation of the framework where the age domain is discretized with finite time steps. Defining $S(t)$ as the total storage at time t, we note that $S(t)p_S(T,t)dT$ represents the volume of water injected in the system around $t - T$ which is still inside the control volume at time t. Notice that if at $t - T$ no input occurred, $p_S(T,t) = 0$. Figure 2b shows the residence time cumulative distribution $P_S(T,t)$ which allows the transformation of variable $T \mapsto P_S$. The distribution $\overleftarrow{\omega}_Q(P_S,t)$ (Figure 2d) prescribes the age-selection processes occurring in discharge formation. The function $\overleftarrow{\omega}_Q(P_S,t)$ can hardly be directly measured because this would imply labeling with different tracers all the different ages contained in the control volume. Therefore, the shape of this distribution needs to be assumed and possibly calibrated. In this example, Q preferentially selects high values of P_S, i.e., the older water in storage. As $\overleftarrow{\omega}_Q(P_S(T,t),t)$ is a derived distribution, the following relation holds: $\overleftarrow{\omega}_Q(P_S,t)dP_S = \overleftarrow{p}_Q(T,t)dT$. Therefore, the solid blue area in Figures 2d and 2c represents the probability that a water particle with age around T_1 is sampled for contributing to the outflow $Q(t)$ at time t. Repeating this procedure for all the age intervals in storage allows a proper computation of the backward TTD in the age domain ($\overleftarrow{p}_Q(T,t)$, Figure 2c). Note that even if $\overleftarrow{\omega}_Q(P_S,t)$ is smooth and regular, the corresponding backward TTD $\overleftarrow{p}_Q(T,t)$ is highly irregular due to the irregular shape of the RTD, which mirrors the time variability of input and output fluxes. Finally, the quantity $Q(t)\overleftarrow{p}_Q(T,t)/S(t)$ (blue shaded bars in Figure 2a) represents the fraction of storage with a certain age that is routed to the discharge flow per unit time. An analogous procedure (Figures 2e and 2f) can be implemented to compute the age distribution of particles that are evapotranspired. In the displayed example, evapotranspiration preferentially selects young water. The difference between how the two output fluxes select different ages is evident in Figure 2a where it can be seen that Q is mainly composed by old water while ET by new one. Different choices of $\overleftarrow{\omega}_Q(P_S,t)$ and $\overleftarrow{\omega}_{ET}(P_S,t)$ allow modeling different age-selection schemes flexibly.

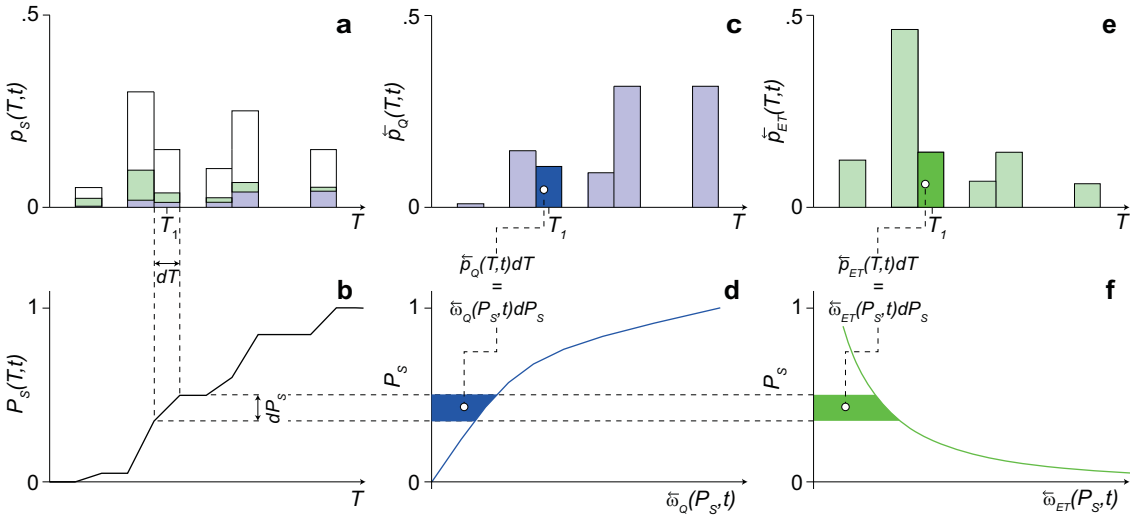

Figure 2. Graphical representation of the modeling scheme. For this representation, we have assumed $dt = 1$. See detailed description on the main text.

2.3. Solute Transport

The framework described in section 2.2 deals with transport and mixing processes of water particles within a hydrologic control volume and can be readily generalized to describe transport of solutes. If the tracer in focus is ideal (i.e., it undergoes the same transport processes as the water carrier without degradation, chemical, physical, or biological reactions or evapoconcentration), the concentration C_J of a parcel of water injected in the system would travel unaltered and the concentration C_Q in the discharge would be straightforwardly derived as

$$C_Q(t) = \int_0^\infty C_J(t-\tau)\overleftarrow{p}_Q(\tau,t)d\tau\,. \tag{3}$$

In equation (3), C_Q is expressed as a weighted average of the concentrations of the water parcels within the system where the weight is the relative fraction of outflow that is sampled from each parcel—the backward TTD. However, ideal tracers do not exist. In fact, even passive tracers can exhibit a resistance to being selected by transpiration (e.g., in case they are toxic to plants). This different resistance can cause an enrichment of solute concentration (evapoconcentration) as a parcel travels through the system [*Bertuzzo et al.*, 2013; *Hrachowitz et al.*, 2013]. As the framework presented in section 2.2 tracks the fate of every particle of water traveling through the system, evapoconcentration can be directly accounted for. Moreover many tracers can undergo decay/degradation under field conditions. A general approach is achieved by defining $C(T, t)$ as the solute concentration at time t of the water input injected at time $t - T$ and by assuming that the concentration of water evapotranspired from such water input is $\alpha C(T,t)$, with $\alpha \in [0,1]$ [*Bertuzzo et al.*, 2013]. The two extreme cases are $\alpha \equiv 0$, where no solute is selected and $\alpha \equiv 1$, where the solute has the same affinity of the water to be transpired. Whenever $\alpha < 1$, solute concentration changes with time. In addition to this physical process, we account also for a linear degradation at a rate k which fairly well describes the behavior of mass loss rates in the soil of many solutes of practical interest. By coupling mass balances of water and solute of single water pulses, the evolution of the concentration becomes (Appendix A)

$$C(T,t) = C_J(t-T)\exp\left[(1-\alpha)\int_0^T \frac{ET(t-T+\tau)\overleftarrow{p}_{ET}(\tau,t-T+\tau)}{S(t-T+\tau)p_S(\tau,t-T+\tau)}d\tau - kT\right], \tag{4}$$

which allows generalizing equation (3) to the case of solutes that undergo evapoconcentration:

$$C_Q(t) = \int_0^\infty C(\tau,t)\overleftarrow{p}_Q(\tau,t)d\tau\,. \tag{5}$$

The algorithm used for the numerical implementation of equations (4) and (5) is described in Appendix A.

2.4. Application to the Tracer Experiments

The extensive analyses carried out in the companion paper [*Queloz et al.*, 2015] suggest that, besides bottom outflow, there are two other possible export pathways for tracer mass: plant uptake and microbial degradation. All these processes can be modeled using the framework developed in section 2.3.

Because of the marked differences between the relevant physical properties of the lysimeter components, we conceptualize the system as a series of two control volumes, the soil and the gravel filter (Figure 1). As the geotextile placed between the soil and the filter (Figure 1) prevents willow roots to penetrate into the filter, *ET* from the filter can be assumed to be null. Moreover, the lysimeter setup [*Queloz et al.*, 2015] does not allow changes in water storage of the filter (unless resorting to unreasonable storativity changes), so we can assume that filter recharge, here termed L, is equal to bottom outflow, termed Q, at every time (Figure 1). Under such assumption, all water storages, input and output fluxes of the two control volumes (i.e., $S(t)$, $J(t)$, $ET(t)$, $L(t)$, and $Q(t)$, Figure 1b) are known from the measurements carried out. We first apply the model described in sections 2.2 and 2.3 to the soil control volume forced by the precipitation input $J(t)$ with tracer concentration $C_J(t)$ to compute the concentration $C_L(t)$ of tracer in the filter recharge $L(t)$. We then model transport processes in the gravel filter assuming as input the flux $L(t)$ with concentration $C_L(t)$ and compute the concentration $C_Q(t)$ in the bottom outflow.

To apply the model, SAS functions $\overleftarrow{\omega}\,(P_S, t)$ must be specified. We select them among a suite of (time-invariant) power law functions: $\overleftarrow{\omega}_Q(P_S) = \beta P_S^{\beta-1}$. For $\beta > 1$ ($\beta < 1$), the outgoing flux has a preference for older (younger) ages, see e.g., Figure 2d (2f); $\beta = 1$ corresponds to the random sampling scheme where ages are sampled according to their relative abundance in the control volume. This formulation is parsimonious yet flexible and is able to model a wide range of age-selection behaviors.

The breakthrough curve of a single tracer is hence completely determined by five parameters: β_{ET}, β_L, β_Q (the exponents of the SAS functions corresponding to the outgoing fluxes *ET* and L from the soil volume and of the outflux Q from the filter, respectively), the affinity to be evapotranspired α and the degradation rate k. To ease the interpretation of the results, in the following we will refer to the half-life of the solute $DT_{50} = (\ln 2)/k$. When multiple tracers are modeled simultaneously, each solute i is possibly characterized by different parameters α_i and $DT_{50,i}$, leading to a total number of 13 parameters in this study.

We use a Monte Carlo approach to calibrate the parameters contrasting measured and modeled time series of mean daily concentrations of the five tracers in the discharge. A criterion based on the residual sum of squares (RSS) is used to select the behavioral simulations [in the sense of *Beven*, 2012] which are used to plot the results. Further details are provided in Appendix B. The model is validated using data pertaining a subsequent injection of two out of five tracers (Figure 1b).

3. Results

Frequency distributions of behavioral parameter sets are reported in Figure 3. The corresponding modeled breakthrough curves and fractions of exported mass for the five tracers are compared to measured data in Figure 4. The very different patterns of transport exhibited by the five marked injections are quite well captured by the model.

Parameter distributions (Figure 3) reveal that the exponents of the backward TTD related to the soil control volume (β_L and β_{ET}) are clearly identified, while model results are less sensitive to variations of age-selection processes in the gravel filter (β_Q). Inferred backward TTDs indicate that *ET* has a clear preference for young water ($\beta_{ET} < 1$), while discharge for old water ($\beta_L > 1$). The distribution of β_Q is wider, such that no clear age-selection patterns emerge. The mean value of β_Q is 1.51, relatively close to a random sampling scheme ($\beta = 1$). Parameters describing the affinity to be transpired and degradation processes (i.e., α_i and $DT_{50,i}$) could not be clearly identified because different combinations of the two processes, both representing possible sinks of tracer mass, can lead to similar export dynamics. The breakthrough curves of tracers 2, 4, and 5 can be explained not only by an almost conservative behavior (i.e., negligible degradation, high $DT_{50,i}$) and high affinities (i.e., α_i close to 1) but also by progressively shorter half-lives (of the order of a hundred days) and lower affinities (Figure 3b). Long half-lives could not be clearly identified because, given the time scale of the experiment, any $DT_{50,i}$ longer than a thousand days leads to indistinguishable outcomes. Tracer 1 never broke through the bottom outflow. This null export can be explained either by fast degradation or

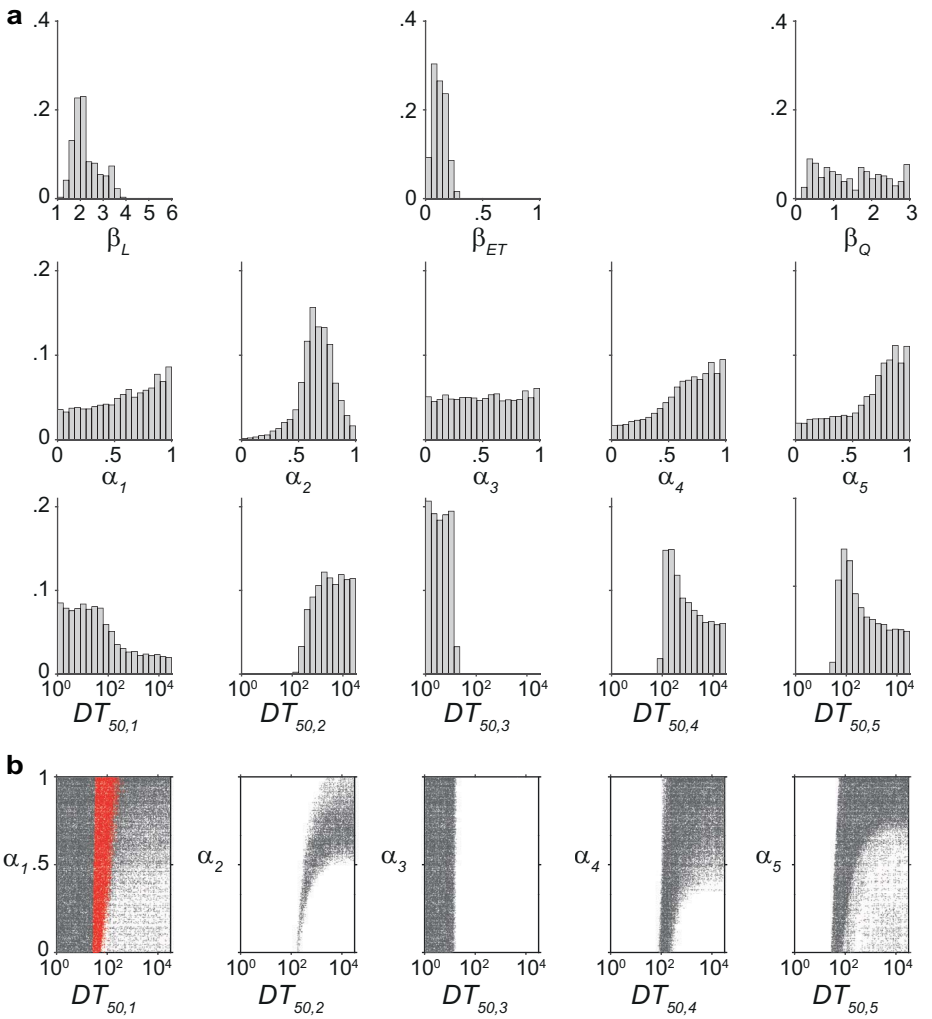

Figure 3. (a) Frequency distributions of behavioral parameter sets. (b) Scatter plot of behavioral pairs of parameters α_i and $DT_{50,i}$. Red dots in the first subplot indicate behavioral pairs (α_1, $DT_{50,1}$) obtained using also the information collected in the second injection of tracer 1. $DT_{50,i}$ is expressed in days.

by a combination of conservative behavior and plant uptake. On the contrary, the almost null export of tracer 3 can be reproduced only by assuming a short half-life. As opposed to all other tracers, its behavior cannot be explained only by assuming plant uptake and no degradation.

Even though the peaks of the observed breakthrough curves (Figure 4, top) are not perfectly reproduced in some cases (e.g., tracer 4), their timing is well captured by the model. Similarly, the timing of the first sharp increase of fluorobenzoic acid concentration is well reproduced. The temporal evolution of the fraction of mass recovered in the discharge (Figure 4, bottom) is also well reproduced for all tracers. For comparison, Figure 4 also reports the hypothetical export dynamics of an ideal tracer (i.e., $\alpha = 1$ and $DT_{50} = \infty$) and of a conservative tracer which is not subject to plant uptake (i.e., $\alpha = 0$ and $DT_{50} = \infty$). The mass flux of an ideal tracer in the outflow is proportional to the forward TTD and, as such, it depends on the time of injection. Indeed, the total mass exported at the end of the experiment is rather different for the five injections considered (red-dashed lines in Figure 4b). The behavior of an ideal tracer, which perfectly tracks the transport of water, is compatible with that of all tracers but tracer 3. No plant uptake ($\alpha = 0$) causes evapoconcentration of the tracer and leads to higher breakthrough curves and fractions of recovered mass close to unity by the end of the experiment (green-dashed lines in Figure 4).

The selected behavioral parameter sets are used to model the simultaneous reinjection of tracers 1 and 4 (occurred when previously injected tracers were no longer detectable in the system, Figure 1b) without

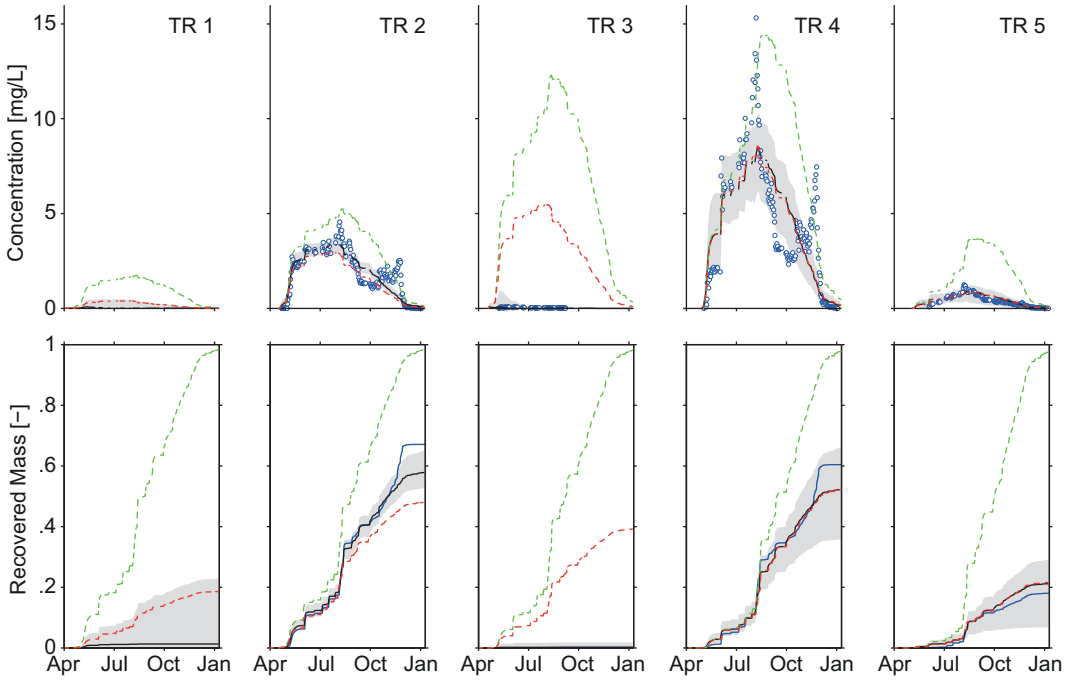

Figure 4. (top) Comparison between simulated and measured breakthrough curves and (bottom) fractions of injected mass retrieved in the bottom outflow for the five tracers (columns). Blue circles and blue lines represent the measured data. Black lines and gray shaded areas show the medians and the 5–95 percentile ranges of the behavioral simulations, respectively. Red and green dashed lines show the median behavior of an ideal tracer (i.e., $\alpha = 1$ and $DT_{50} = \infty$) and of a conservative tracer which is not subject to plant uptake (i.e., $\alpha = 0$ and $DT_{50} = \infty$), respectively.

further calibration. Results of this validation analysis are reported in Figure 5. These two tracers exhibited very different dynamics during the first injection: tracer 1 was never recovered at the outlet while tracer 4 had the highest fraction of exported mass (Figure 4). When injected simultaneously, the two tracers show similar patterns (Figure 5). These very different behaviors, which depend on the different hydrologic forcings occurred during the experiments, can be reproduced by the model. However, the wide distributions of behavioral parameters α_1 and $DT_{50,1}$ lead to a wide spectrum of possible outcomes for the modeled export of tracer 1. Using also the information gathered in the reinjection of tracer 1 in the calibration phase, it is possible to better identify the parameters α_1 and $DT_{50,1}$ (red dots in Figure 3b).

While experimental data allows us to estimate transport dynamics only for the marked injections, a model calibrated on measured data allows inferring the hydrologic history of every component of the storage. Figure 6 presents an overview of the time evolution of hydrological variables and of the RTD and forward and backward TTDs. For the sake of simplicity, we refer to a single control volume: the soil component of the lysimeter (Figure 1a). Oblique lines in Figure 6c show pairs of t and T such that at $t - T$ an injection occurred and thus RTDs and backward TTDs are greater than 0. Following these oblique lines, one can see the evolution of the relative contribution of a water input (injected at the intersection with the x axis) to the storage ($p_S(T,t)$), the outflow flux ($\overleftarrow{p}_L(T,t)$) and the evapotranspiration flux ($\overleftarrow{p}_{ET}(T,t)$). Forward TTDs (Figure 6d) are instead defined for all ages but only for times when an injection took place. The different age-selection processes occurring in the formation of Q and ET result in very different mean travel times: around 70 days for Q and 10 for ET (Figure 6f). Note how the means of forward and backward TTDs differ. When outflow is null, e.g., between 24 September and 12 October, $\overleftarrow{p}_L(T,t)$ and the corresponding mean are not defined.

The time window displayed in Figure 6 spans from August to December to highlight the different transport dynamics induced by the different magnitudes of ET (Figure 6b). During winter (low ET), the fraction of precipitation that will leave the system through outflow ($\theta(t_i)J(t_i)$, blue bars in Figure 6a) dominates, while it is reduced during summer. In such period a water particle is more likely to exit through the outflow. As a consequence, the mean forward travel time (the mean travel time of all particles injected at a certain time) is lower (Figure 6f). It can be noticed how large rainfall events reduce mean residence time by bringing young

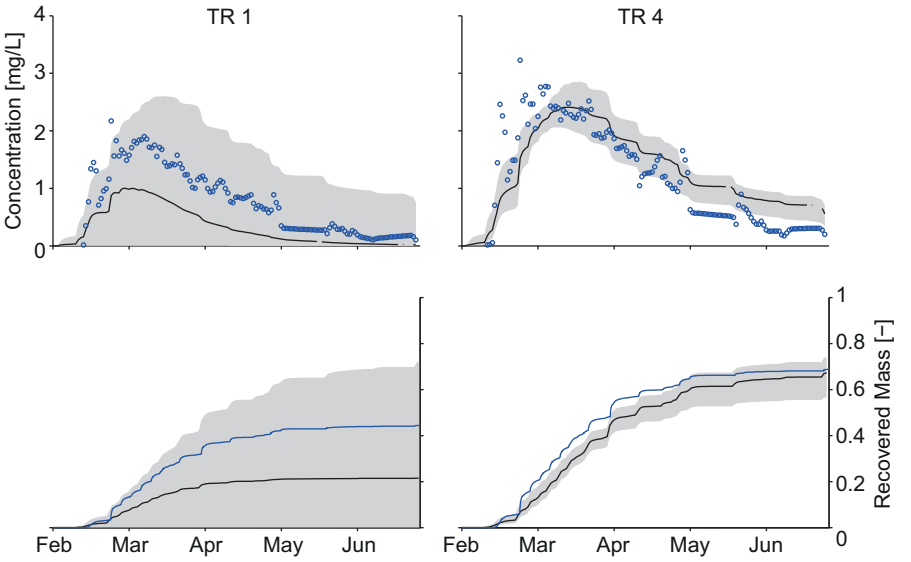

Figure 5. Validation of model results. (top) Comparison between simulated and measured breakthrough curves and (bottom) fractions of injected mass retrieved in the bottom outflow for the reinjection of tracers 1 and 4. Symbols as in Figure 3. Model results are obtained using the behavioral parameter sets obtained in the first experiment (Figure 3) without further calibration.

water (with age equal to zero) into the system. The time evolution of the outflow mean backward travel time (the mean travel time of all particles exiting as L at a certain time) follows closely that of the mean residence time ($r = 0.95$), indicating that, although outflow samples preferentially old water, the average age is controlled by the availability of ages in storage.

4. Discussion

The results presented suggest that the large variance exhibited by the transport dynamics of tracers 1, 2, 4, and 5 can be explained by the behavior of an ideal tracer which tracks water transport features, including transpiration, without degrading. Under these conditions, the fate of the water inputs marked with different tracers is determined by the hydrologic signal faced by the water parcels while traveling through the system. This is also supported by the results of the model validation. When the tracers are injected simultaneously, they exhibit similar transport behaviors. This provides strong experimental evidence, supported by a robust theoretical framework, of the nonstationary character of travel time distributions.

While the initial five injections of tracer occurred within 1 month, release in the outflow lasted for almost 9 months. Therefore, a large fraction of the hydrologic conditions experienced by the marked injections were identical. This result suggests that, in the actual system, the conditions faced immediately after injection are crucial to determine the overall fraction of water that will leave the system through discharge outflow. In particular, the role of plant uptake for hydrochemical balance cannot be underestimated when analyzing TTDs at any scales. Plants are able to transpire a large fraction of soil water. The amount of water withdrawn, the presence of possible fractionation processes or the age distribution of water particles incorporated by plants may bear profound effects on catchment-scale transport features. In our modeling exercise, the fitted parameters indicate that ET samples preferentially new water, while Q samples older water. This result was somewhat expected given the predominantly vertical nature of the flow in the lysimeter. At catchment scales, different results could be expected. Surface and subsurface subhorizontal flows or macropores can rapidly convey a large amount of event water to the outlet, possibly increasing the relative importance of new water in the catchment-scale backward TTD, particularly during high flows [*van der Velde et al.*, 2012; *Benettin et al.*, 2013a]. Moreover, significant geomorphological complexity, say epitomized by catchment width functions (the relative proportion of injection sites equally distant from the outlet), are known to impact mixing and sampling patters, possibly resulting in higher degrees of mixing between different ages in stream waters.

The results presented in Figure 6 show that even time-invariant SAS functions produce time-variant transport features (e.g., mean travel times) depending on the state of the system (i.e., the storage) and on the

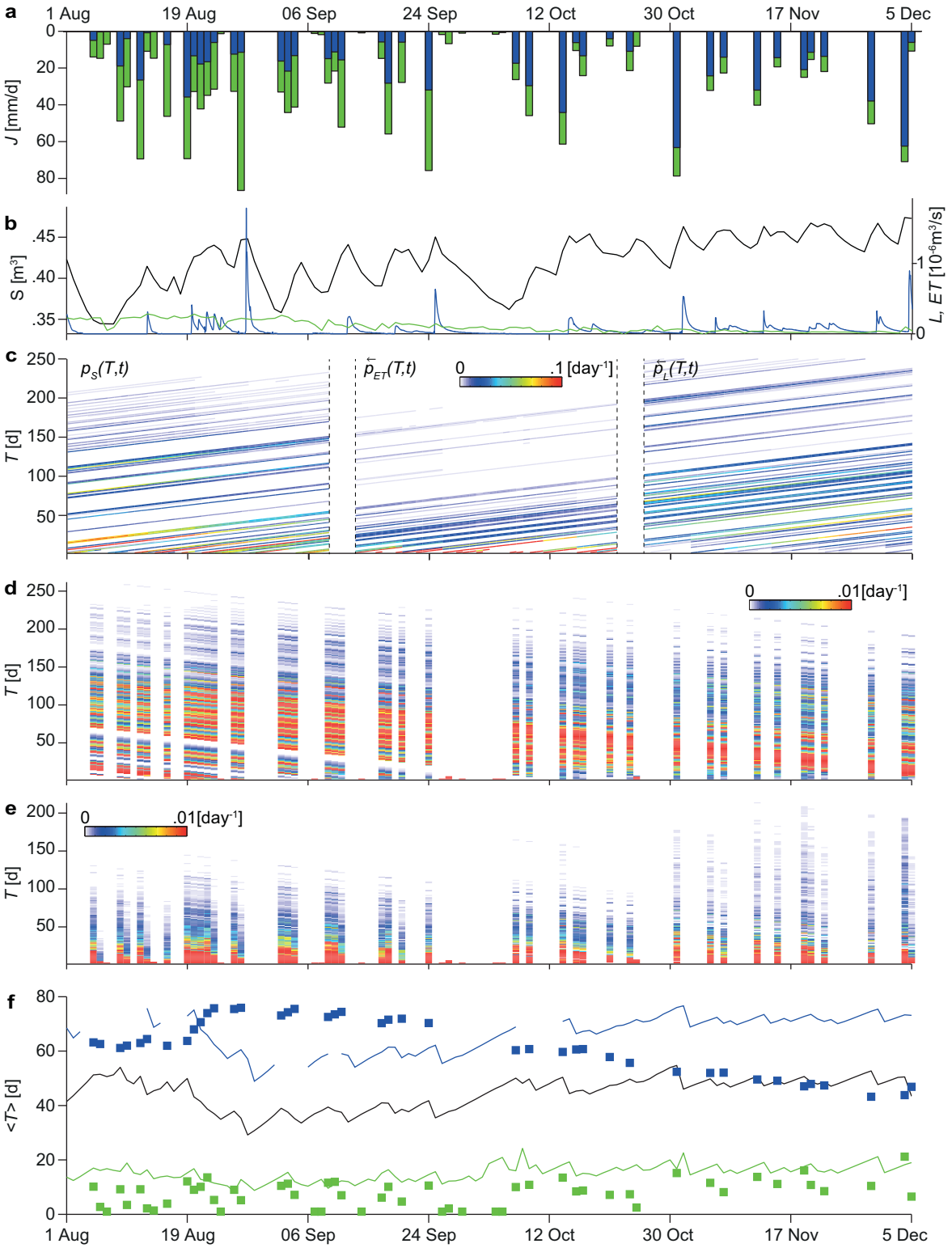

Figure 6. Summary of relevant distributions in the soil control volume. (a) Time series of rainfall, fraction of rainfall inputs that will leave the system through outflow L ($\theta(t)J(t)$, blue bars) and ET ($(1-\theta(t))J(t)$, green bars). (b) Time series of water storage S (black), outflow L (blue), and ET (green). Colors in Figure 6c show RTD $p_S(T,t)$, backward TTDs $\overleftarrow{p}_{ET}(T,t)$, and $\overleftarrow{p}_L(T,t)$ as a function of age (y axis) and time (x axis). Analogously, the forward TTDs $\vec{p}_L(T,t)$ and $\vec{p}_{ET}(T,t)$ are displayed in Figures 6d and 6e, respectively. (f) Time series of mean residence time (black line), mean outflow (blue), and ET (green) travel times for forward (squares) and the backward (lines) distributions. Distributions are calculated with $\beta_L=2$ and $\beta_{ET}=0.2$. To achieve precise estimates of the variables displayed, we have synthetically extended the duration of the data set available up to 3 years repeating three times the observed time series of hydrological variables (May 2013 to May 2014), one before and one after the actual experimental period.

external forcings (i.e., the evapotranspiration rate). We have also tested more complex, time-variant age-selection schemes obtained assuming that the exponents β vary linearly with water storage, similarly to *Harman* [2015]. No significant improvement was found for the lysimeter experiment. Nonetheless, it will be interesting to test this hypothesis in more complex settings.

5. Conclusions

There is a growing consensus in the hydrologic community that collection of hydrologic data should be complemented with measurements of tracers to properly understand how water moves through catchments [*McDonnell and Beven*, 2014]. This calls for simple, flexible, and commonly accepted tools to interpret tracer data in terms of residence and travel time distributions. We believe that the framework presented herein fulfills such requirements.

Overall the results presented show that a framework for hydrologic transport based on time-variant travel time distributions is able to explain the nonstationary behavior exhibited by experimental data of tracer transport in a large lysimeter. Although the scale of the experiment is small compared to that of hillslopes and catchments, our approach relies solely on input and output fluxes and thus general guidelines for the application at larger scales can be drawn. The precise knowledge of the lysimeter structure allowed us to identify two separate control volumes (the soil and the gravel filter). At larger scales, however, clear structures and boundaries can hardly be identified, let alone measured. At first instance, one could resort to a single control volume to assess residence and travel time distributions from tracer data. In this case heterogeneity of flow paths, source areas and mixing in catchment storage are charged to the storage selection functions. The application of the method needs the further specification of the time series of all hydrological fluxes and of the storage. While the experimental setup allows the perfect knowledge of all fluxes, in real-life applications, they would need to be measured (precipitation and discharge) or estimated through suitable models (evapotranspiration). Once all fluxes are reasonably estimated, the storage inside the control volume can be inferred via mass balance up to an additive constant: the initial storage, which represents a crucial model parameter controlling the volume of water potentially available for mixing. If simple power law SAS functions of the type introduced in section 2.4 are to be employed, the model requires the calibration of three additional parameters: namely β_{ET}, β_Q, and the coefficient α for the tracer in focus. For the latter, the type of tracer (e.g., chloride and water isotopes) and information about land use and vegetation cover can be used to constrain the *prior* distribution of this parameter. If the tracer is expected to undergo nonnegligible degradation at time scales comparable with the mean travel time, such process can be accounted for at the cost of an additional parameter. However, as highlighted also by the results presented herein, degradation may hamper parameter identification. Therefore, the analysis of conservative tracers is suggested to be more informative for characterizing transport processes. As displayed in Figure 6, the calibrated model allows estimating in retrospect the time evolution of mean residence time and mean forward and backward travel time for both discharge and evapotranspiration in a framework that consistently accounts for nonstationary behaviors.

The procedure outlined assumes that the hydrologic forcings (precipitation, discharge, and evapotranspiration) are either measured or estimated and that they are directly used as inputs for the transport model. This allows a quick interpretation of tracer data in terms of residence and travel time distributions. However, more complex schemes can be envisioned where the hydrologic and the transport models (possibly with multiple control volumes) are coupled. It has been shown that the simultaneous calibration of such models against flow and tracer data allows reducing the uncertainties on the underlying hydrological processes [see e.g., *Fenicia et al*., 2010; *McMillan et al*., 2012; *Bertuzzo et al*., 2013; *Hrachowitz et al*., 2013].

When *Botter et al*. [2010] first introduced the framework adopted herein for time-variant travel time distributions, one critical point that immediately emerged was that a proper characterization of the distribution of the age of water in the discharge cannot be decoupled from the characterization of the age distribution in the evapotranspiration flux. However, directly measuring proxies of evapotranspiration age can experimentally prove hard even at plot scale. Our modeling exercise shows that, as evapotranspiration modifies the availability of ages in storage possibly sampled by discharge, it is possible to infer how evapotranspiration samples the storage from measurements of discharge age composition. This has been suggested at the lysimeter scale; however, the same approach can arguably be applied to any upscaled control volume.

Appendix A: Details on Analytical and Numerical Methods

Let us term $s(T,t)dT = S(t)p_S(T,t)dT$ the volume of water of residence time around T present in the system at time t. $s(T, t)$ is the solution of the following partial differential equation [*Botter et al.*, 2011; *van der Velde et al.*, 2012; *Benettin et al.*, 2013a]:

$$\frac{\partial s(T,t)}{\partial t} + \frac{\partial s(T,t)}{\partial T} = -Q(t)\overleftarrow{p}_Q(T,t) - ET(t)\overleftarrow{p}_{ET}(T,t)\,, \tag{A1}$$

with boundary conditions $s(0,t) = J(t)$. In equation (A1), the variation in time of $s(T, t)$ is expressed in terms of aging (second term of the left-hand side) and removal by Q and ET (right-hand side). The partial differential equation (A1) can be reduced to a family of ordinary differential equations by looking at the solution along characteristic curves of the type $(T(z), t(z))$. Curves of the type $T(z) = z$ and $t(z) = z + t_i$ are characteristics, as revealed by the following equation:

$$\frac{ds(z, z+t_i)}{dz} = \frac{\partial s(T,t)}{\partial T}\frac{dT}{dz} + \frac{\partial s(T,t)}{\partial t}\frac{dt}{dz} = \frac{\partial s(T,t)}{\partial t} + \frac{\partial s(T,t)}{\partial T}\,. \tag{A2}$$

Combining equations (A1) and (A2) and using the relations $T = z$ and $t = z + t_i = T + t_i$, we finally obtain

$$\frac{ds(T, T+t_i)}{dT} = -Q(T+t_i)\overleftarrow{p}_Q(T, T+t_i) - ET(T+t_i)\overleftarrow{p}_{ET}(T, T+t_i)\,, \tag{A3}$$

with initial condition $s(0, t_i) = J(t_i)$. Equation (A3) describes how the volume of a pulse of water injected in the system at time t_i evolves while aging. The difference between the approaches of equations (A1) and (A3) is similar to the difference between Eulerian and Lagrangian approaches, the focus being the residence time rather than the spatial position. Equation (A1) focuses on a particular residence time T and follows different water pulses aging through that residence time. On the contrary, equation (A3) follows the fate of a single water pulse aging inside the system.

Analogously, the time evolution of the mass of solute $m(T, t = T + t_i)dT$ carried by the water pulse entered around t_i can be derived as

$$\begin{aligned} \frac{dm(T, T+t_i)}{dT} &= \frac{d(s(T, T+t_i)C(T, T+t_i))}{dT} = \\ &= -C(T, T+t_i)[Q(T+t_i)\overleftarrow{p}_Q(T, T+t_i) + \alpha ET(T+t_i)\overleftarrow{p}_{ET}(T, T+t_i)] - kT\,, \end{aligned} \tag{A4}$$

with initial condition $m(0, t_i) = J(t_i)C_J(t_i)$. In equation (A4), $C(T, T+t_i)$ represents the solute concentration of the water pulse while $\alpha C(T, T+t_i)$ is the concentration in the evapotranspiration flux. The term $-kT$ at the RHS accounts for degradation. Coupling equations (A3) and (A4) and solving for $C(T, T+t_i)$, the solution 4 reported in section 2.3 is straightforwardly derived.

From a numerical viewpoint, first the sequence of injections is discretized at hourly time step, then the evolution of the volume and of the solute mass of every single pulse of water are computed by integrating equations (A3) and (A4). At any time, the backward TTDs $\overleftarrow{p}_{ET}(T,t)$ and $\overleftarrow{p}_Q(T,t)$ are computed as explained in section 2.2 based on the current RTD $p_S(T,t) = s(T,t)/S(t)$.

Water stored in the two control volumes at the beginning of the experiment ($t = 0$, the injection of the first tracer) needs to be accounted for in the simulation. This is done by considering that, at any time t, the initial storage is older than t, and therefore contributes to the output fluxes as prescribed by the corresponding backward TTDs (i.e., with probability $\int_{P_S(t,t)}^{1} \overleftarrow{\omega}(x,t)dx$).

Appendix B: Model Calibration

Parameters are calibrated by contrasting measured and modeled time series of mean daily concentrations of the five tracers at the lysimeter outlet. We use a Monte Carlo approach randomly selecting 10^4 sets of parameters controlling TTDs (β_{ET}, β_L, β_Q) from uniform distributions with ranges illustrated in Figure 3a. For each parameter set and for each tracer i, we test 400 pairs of parameters α_i and $\log_{10}(DT_{50,i})$ randomly selected in the intervals [0,1] and [0,4.5], respectively. As the breakthrough curves exhibit very different behaviors, we first normalize each time series of concentration dividing it by its maximum value for all tracers but 1 and 3, which show null or negligible export. The performance of each simulation is evaluated through the residual sum of squares (RSS_i).

For each tracer i, a set of parameters (β_{ET}, β_L, β_Q, α_i, $DT_{50,i}$) is considered behavioral [in the sense of *Beven*, 2012] if $RSS_i < A$, where A is a suitable threshold, and the subset of parameters controlling the TTDs (β_{ET}, β_L, β_Q) is able to achieve a good performance also for all other tracers ($RSS_j < C \forall j \neq i$). The latter constraint is imposed because, while tracers can have specific properties (i.e., α_i, $DT_{50,i}$), water carrying them is obviously subject to the same transport processes. The threshold A is arbitrarily fixed to 5, a value that corresponds to an error that we deem acceptable.

Acknowledgments
The authors thank the Swiss National Science Foundation (SNF) for funding through the research project 135241. Data available as supporting information of the companion paper [*Queloz et al.*, 2015]. P.Q. and L.C. contributed equally to this work.

References

Ali, M., A. Fiori, and D. Russo (2014), A comparison of travel-time based catchment transport models, with application to numerical experiments, *J. Hydrol.*, *511*, 605–618.
Benettin, P., Y. van der Velde, S. E. A. T. M. van der Zee, A. Rinaldo, and G. Botter (2013a), Chloride circulation in a lowland catchment and the formulation of transport by travel time distributions, *Water Resour. Res.*, *49*, 4619–4632, doi:10.1002/wrcr.20309.
Benettin, P., A. Rinaldo, and G. Botter (2013b), Kinematics of age mixing in advection-dispersion models, *Water Resour. Res.*, *49*, 8539–8551, doi:10.1002/2013WR014708.
Bertuzzo, E., M. Thomet, G. Botter, and A. Rinaldo (2013), Catchment-scale herbicides transport: Theory and application, *Adv. Water Resour.*, *52*, 232–242.
Beven, K. (2012), *Rainfall-Runoff Modelling: The Primer*, 2nd ed., 457 pp., John Wiley, Chichester, U. K.
Birkel, C., C. Soulsby, D. Tetzlaff, S. Dunn, and L. Spezia (2012), High-frequency storm event isotope sampling reveals time-variant transit time distributions and influence of diurnal cycles, *Hydrol. Processes*, *26*(2), 308–316.
Botter, G. (2012), Catchment mixing processes and travel time distributions, *Water Resour. Res.*, *48*, W05545, doi:10.1029/2011WR011160.
Botter, G., E. Bertuzzo, A. Bellin, and A. Rinaldo (2005), On the Lagrangian formulations of reactive solute transport in the hydrologic response, *Water Resour. Res.*, *41*, W04008, doi:10.1029/2004WR003544.
Botter, G., E. Milan, E. Bertuzzo, S. Zanardo, M. Marani, and A. Rinaldo (2009), Inferences from catchment-scale tracer circulation experiments, *J. Hydrol.*, *369*(34), 368–380.
Botter, G., E. Bertuzzo, and A. Rinaldo (2010), Transport in the hydrologic response: Travel time distributions, soil moisture dynamics, and the old water paradox, *Water Resour. Res.*, *46*, W03514, doi:10.1029/2009WR008371.
Botter, G., E. Bertuzzo, and A. Rinaldo (2011), Catchment residence and travel time distributions: The master equation, *Geophys. Res. Lett.*, *38*, L11403, doi:10.1029/2011GL047666.
Broxton, P. D., P. A. Troch, and S. W. Lyon (2009), On the role of aspect to quantify water transit times in small mountainous catchments, *Water Resour. Res.*, *45*, W08427, doi:10.1029/2008WR007438.
Brutsaert, W., and J. L. Nieber (1977), Regionalized drought flow hydrographs from a mature glaciated plateau, *Water Resour. Res.*, *13*(3), 637–644.
Cvetkovic, V., C. Carstens, J.-O. Selroos, and G. Destouni (2012), Water and solute transport along hydrological pathways, *Water Resour. Res.*, *48*, W06537, doi:10.1029/2011WR011367.
Dagan, G. (1988), *Flow and Transport in Porous Formations*, 257 pp., Springer, N. Y.
Davies, J., K. Beven, A. Rodhe, L. Nyberg, and K. Bishop (2013), Integrated modeling of flow and residence times at the catchment scale with multiple interacting pathways, *Water Resour. Res.*, *49*, 4738–4750, doi:10.1002/wrcr.20377.
Fenicia, F., S. Wrede, D. Kavetski, L. Pfister, L. Hoffmann, H. H. G. Savenije, and J. J. McDonnell (2010), Assessing the impact of mixing assumptions on the estimation of streamwater mean residence time, *Hydrol. Processes*, *24*(12), 1730–1741.
Haggerty, R., S. M. Wondzell, and M. A. Johnson (2002), Power-law residence time distribution in the hyporheic zone of a 2nd-order mountain stream, *Geophys. Res. Lett.*, *29*(13), doi:10.1029/2002GL014743.
Harman, C. (2015), Time-variable transit time distributions and transport: Theory and application to storage-dependent transport of chloride in a watershed, *Water Resour. Res.*, *51*, 1–30, doi:10.1002/2014WR015707.
Harman, C. J., and M. Kim (2014), An efficient tracer test for time-variable transit time distributions in periodic hydrodynamic systems, *Geophys. Res. Lett.*, *41*, 1567–1575, doi:10.1002/2013GL058980.
Heidbuchel, I., P. A. Troch, S. W. Lyon, and M. Weiler (2012), The master transit time distribution of variable flow systems, *Water Resour. Res.*, *48*, W06520, doi:10.1029/2011WR011293.
Heidbüchel, I., P. A. Troch, and S. W. Lyon (2013), Separating physical and meteorological controls of variable transit times in zero-order catchments, *Water Resour. Res.*, *49*, 7644–7657, doi:10.1002/2012WR013149.
Hrachowitz, M., C. Soulsby, D. Tetzlaff, J. J. C. Dawson, S. M. Dunn, and I. A. Malcolm (2009), Using long-term data sets to understand transit times in contrasting headwater catchments, *J. Hydrol.*, *367*(34), 237–248.
Hrachowitz, M., C. Soulsby, D. Tetzlaff, I. A. Malcolm, and G. Schoups (2010), Gamma distribution models for transit time estimation in catchments: Physical interpretation of parameters and implications for time-variant transit time assessment, *Water Resour. Res.*, *46*, W10536, doi:10.1029/2010WR009148.
Hrachowitz, M., H. Savenije, T. A. Bogaard, D. Tetzlaff, and C. Soulsby (2013), What can flux tracking teach us about water age distribution patterns and their temporal dynamics?, *Hydrol. Earth Syst. Sci.*, *17*(2), 533–564.
Jury, W. A., G. Sposito, and R. E. White (1986), A transfer-function model of solute transport through soil. 1. Fundamental-concepts, *Water Resour. Res.*, *22*(2), 243–247.
Kirchner, J. W. (2009), Catchments as simple dynamical systems: Catchment characterization, rainfall-runoff modeling, and doing hydrology backward, *Water Resour. Res.*, *45*, W02429, doi:10.1029/2008WR006912.
Kirchner, J. W., and C. Neal (2013), Universal fractal scaling in stream chemistry and its implications for solute transport and water quality trend detection, *Proc. Natl. Acad. Sci. U. S. A.*, *110*(30), 12,213–12,218.
Kirchner, J. W., X. Feng, and C. Neal (2000), Fractal stream chemistry and its implications for contaminant transport in catchments, *Nature*, *403*(6769), 524–527.
Kreft, A., and A. Zuber (1978), On the physical meaning of the dispersion equation and its solutions for different initial and boundary conditions, *Chem. Eng. Sci.*, *33*(11), 1471–1480.
Maloszewski, P., W. Rauert, P. Trimborn, A. Herrmann, and R. Rau (1992), Isotope hydrological study of mean transit times in an alpine basin (Wimbachtal, Germany), *J. Hydrol.*, *140*(1–4), 343–360.

McDonnell, J. J., and K. Beven (2014), Debates—The future of hydrological sciences: A (common) path forward? A call to action aimed at understanding velocities, celerities and residence time distributions of the headwater hydrograph, *Water Resour. Res.*, *50*, 5342–5350, doi:10.1002/2013WR015141.

McGuire, K. J., and J. J. McDonnell (2006), A review and evaluation of catchment transit time modeling, *J. Hydrol.*, *330*(3–4), 543–563.

McMillan, H., D. Tetzlaff, M. Clark, and C. Soulsby (2012), Do time-variable tracers aid the evaluation of hydrological model structure? A multimodel approach, *Water Resour. Res.*, *48*, W05501, doi:10.1029/2011WR011688.

Niemi, A. J. (1977), Residence time distributions of variable flow processes, *Int. J. Appl. Radiat. Isot.*, *28*(1011), 855–860.

Queloz, P., E. Bertuzzo, L. Carraro, G. Botter, F. Miglietta, P. S. C. Rao, and A. Rinaldo (2015), Transport of fluorobenzoate tracers in a vegetated hydrologic control volume: 1. Experimental results, *Water Resour. Res.*, *51*, doi:10.1002/2014WR016433.

Rinaldo, A., K. J. Beven, E. Bertuzzo, L. Nicotina, J. Davies, A. Fiori, D. Russo, and G. Botter (2011), Catchment travel time distributions and water flow in soils, *Water Resour. Res.*, *47*, W07537, doi:10.1029/2011WR010478.

Rodhe, A., L. Nyberg, and K. Bishop (1996), Transit times for water in a small till catchment from a step shift in the oxygen 18 content of the water input, *Water Resour. Res.*, *32*(12), 3497–3511.

Rodriguez-Iturbe, I., A. Porporato, L. Ridolfi, V. Isham, and D. R. Coxi (1999), Probabilistic modelling of water balance at a point: The role of climate, soil and vegetation, *Proc. R. Soc. London, Ser. A*, *455*(1990), 3789–3805.

Seeger, S., and M. Weiler (2014), Lumped convolution integral models revisited: On the meaningfulness of inter catchment comparisons, *Hydrol. Earth Syst. Sci. Discuss.*, *11*(6), 6753–6803, doi:10.5194/hessd-11-6753-2014.

van der Velde, Y., G. H. de Rooij, J. C. Rozemeijer, F. C. van Geer, and H. P. Broers (2010), Nitrate response of a lowland catchment: On the relation between stream concentration and travel time distribution dynamics, *Water Resour. Res.*, *46*, W11534, doi:10.1029/2010WR009105.

van der Velde, Y., P. J. J. F. Torfs, S. E. A. T. M. van der Zee, and R. Uijlenhoet (2012), Quantifying catchment-scale mixing and its effect on time-varying travel time distributions, *Water Resour. Res.*, *48*, W06536, doi:10.1029/2011WR011310.

van der Velde, Y., I. Heidbuchel, S. W. Lyon, L. Nyberg, A. Rodhe, K. Bishop, and P. A. Troch (2014), Consequences of mixing assumptions for time-variable travel time distributions, *Hydrol. Processes*, doi:10.1002/hyp.10372.